Clim. Past, 21, 79–93, 2025
https://doi.org/10.5194/cp-21-79-2025

Climate of the Past
Open Access
EGU

Southern Ocean control on atmospheric CO_2 changes across late Pliocene Marine Isotope Stage M2

Suning Hou, Leonie Toebrock, Mart van der Linden, Fleur Rothstegge, Martin Ziegler, Lucas J. Lourens, and Peter K. Bijl

Department of Earth Sciences, Utrecht University, 3584 CB Utrecht, the Netherlands

Correspondence: Suning Hou (s.hou@uu.nl)

Received: 1 May 2024 – Discussion started: 13 May 2024
Revised: 29 October 2024 – Accepted: 30 October 2024 – Published: 14 January 2025

Abstract. During the Pliocene, atmospheric CO_2 concentrations (pCO_2) were probably sometimes similar to today's, and global average temperature was $\sim 3\,^{\circ}C$ higher than preindustrial. However, the relationships and phasing between variability in climate and pCO_2 on orbital timescales are not well understood. Specifically, questions remain about the nature of a lag of pCO_2 relative to benthic foraminiferal $\delta^{18}O$ in late Pliocene Marine Isotope Stage (MIS) M2 (3300 ka), which was longer than during the Pleistocene. Here, we present a multiproxy paleoceanographic reconstruction of the late Pliocene subtropical–subantarctic zone. New dinoflagellate cyst assemblage data are combined with previously published sea surface temperature reconstructions to reveal past surface conditions, including latitudinal migrations of the subtropical front (STF) over the late Pliocene at Ocean Drilling Program (ODP) Site 1168, offshore of western Tasmania. We observe strong oceanographic variability at the STF over glacial–interglacial timescales, especially the interval (3320–3260 ka) across MIS M2. By providing tight and independent age constraints from benthic foraminiferal $\delta^{18}O$, we find that, much more than benthic $\delta^{18}O$ or local SST, latitudinal migrations of the STF are tightly coupled to global pCO_2 variations across the M2. Specifically, a northerly position of the STF during the MIS M2 deglaciation coincides with generally low pCO_2. We postulate that the Southern Ocean CO_2 outgassing varied strongly with migrations of the STF and that this in part accounted for the variability in pCO_2 across MIS M2.

1 Introduction

As the largest exogenic carbon reservoir on Earth, the ocean plays a pivotal role in regulating Earth's climate through the balance between CO_2 uptake and outgassing (Friedlingstein et al., 2022; Sabine et al., 2004). Upwelling in the polar frontal zone flushes respired CO_2 from the deep ocean into the atmosphere (Process 1 in Fig. 1a). This process is proposed to be controlled by shifts in sea ice extent and westerlies over glacial and interglacial climates by ocean-only general circulation models (Toggweiler et al., 2006), which move the latitudinal position of oceanic fronts in the Southern Ocean. However, modeling outputs are not always in agreement with each other (Gottschalk et al., 2019) or with geological reconstructions (Rae et al., 2018; Skinner et al., 2010; Venugopal et al., 2023). Hence, significant uncertainties persist in our understanding of ice–ocean–climate interactions. Moreover, the biological carbon pump absorbs dissolved CO_2 and removes it from surface waters via export productivity (Martin, 1990; Martínez-García et al., 2014; Thöle et al., 2019), thereby reducing surface dissolved inorganic carbon (DIC), which enhances CO_2 diffusion from the atmosphere (Processes 2 and 3 in Fig. 1a; Egleston et al., 2010; Gruber et al., 2023). This process mainly takes place at the boundary between the subantarctic and subtropical zone (SAZ), where ocean surface temperature (which has a negative influence on CO_2 uptake), ocean stratification (negative), salinity (negative), and DIC (negative) determine CO_2 diffusion. The SAZ is currently a major carbon sink as a result of both increased anthropogenic emissions and natural ocean circulation (Gruber et al., 2009). The past decades have seen profound changes in sea surface temperature (SST), sea surface salinity (SSS), and the stratification of the SAZ surface

waters (Sabine et al., 2004; Gruber et al., 2023). But how these changes will affect the ability of the ocean to act as a climate change mitigator in the coming decades and the amount of excess CO_2 that would consequently remain in the atmosphere are currently uncertain (Gruber et al., 2023). This creates a critical uncertainty in the projections of atmospheric CO_2 concentration (pCO_2) and the resulting effects on climate and sea level, given emission pathway scenarios (Burton et al., 2023; IPCC, 2019).

Reconstructing Southern Ocean conditions in past deglaciation phases might help in understanding interactions between atmospheric climate and ocean conditions. The late Pliocene is marked by dominant obliquity-controlled benthic foraminiferal oxygen isotope ($\delta^{18}O_{bf}$) increases that have been interpreted as glaciation–cooling phases (e.g., Tiedemann et al., 1994; Shackleton et al., 1995; Lisiecki and Raymo, 2005). The most prominent of these is Marine Isotope Stage (MIS) M2 (3300 ka; Keigwin, 1987), the deglaciation of which terminates in the mid-Piacenzian warm period (mPWP, 3264–3025 ka). Questions remain on the nature of its forcing, but also whether this event is mostly reflective of deep-ocean cooling or ice volume increase. Antarctic ice-proximal lithological and biomarker records suggest surface cooling and ice advance, and therefore ice volume increase is involved (Cook et al., 2013; McKay et al., 2012; Patterson et al., 2014), perhaps also in the Northern Hemisphere as suggested by ice-rafted detritus (Flesche Kleiven et al., 2002). In contrast, bottom water temperature (BWT; Braaten et al., 2023) and ice sheet (Mas e Braga et al., 2023; Yamane et al., 2015) studies suggest limited ice volume change across the M2–mPWP transition.

The subsequent mPWP is the most recent time when climate conditions were at times equilibrated to modern-like pCO_2 of about 400 parts per million (ppm, CenCO2PIP Consortium, 2023; De la Vega et al., 2020), although there are discrepancies between proxies and reconstructions, and few records capture sub-orbital temporal resolution (e.g., Seki et al., 2010). MIS KM5c (3205 ka) has been a particular focal point of study because of the similar orbital and continental configuration as today (Haywood et al., 2020). The Pliocene Model Intercomparison Project Phase 2 (PLIOMIP 2; Haywood et al., 2020) compares an ensemble of numerical models run under similar boundary conditions to global compilations of proxy data from sediment cores (e.g., of sea surface temperature, SST; McClymont et al., 2020). From these efforts, global average sea surface temperature ($\sim 2.3\,^{\circ}C$ warmer than preindustrial; McClymont et al., 2020), equilibrium climate sensitivity to pCO_2 (2.6–4.8 °C; Haywood et al., 2020), and an increased hydrological cycle (wetter equatorial regions, drier subtropical regions; Han et al., 2021) were reconstructed.

The nature of and forcing factors behind the M2–mPWP glacial–interglacial transition (3320–3260 ka) are not well understood. High-resolution pCO_2 reconstructions for the late Pliocene reveal low-amplitude variability on orbital timescales (De la Vega et al., 2020), i.e., of similar magnitude as that in the late Pleistocene, but the trends in pCO_2 and $\delta^{18}O_{bf}$ are not as synchronous as in the Pleistocene. Specifically, while PLIOMIP2 demonstrates that overall high pCO_2 in the late Pliocene is likely responsible for the warmer-than-modern climates (Burton et al., 2023), questions remain on the exact phase relationship between pCO_2 change and $\delta^{18}O_{bf}$ across the M2–mPWP transition. Available records seem to suggest that pCO_2 lags changes in $\delta^{18}O_{bf}$ and (sub)surface cooling by about 10–20 kyr (De la Vega et al., 2020; Van der Weijst et al., 2022) or in any case on these timescales are not directly related through climate sensitivity to radiative forcing. We further note that collective knowledge on high-resolution pCO_2 change across the M2–mPWP interval is restricted to one record from Ocean Drilling Program (ODP) Site 999 in the North Atlantic. Mg / Ca- and clumped isotope-based deep-sea cooling also demonstrates a lag relative to $\delta^{18}O_{bf}$ (Braaten et al., 2023). This leaves the open question of how pCO_2, the ocean, and the cryosphere influenced each other over the M2–mPWP transition.

Here we investigate how the surface oceanography of one of the current major ocean carbon sinks, the SAZ, changed through the M2–mPWP transition and infer the implications for the atmospheric CO_2 uptake of the region. We present a multiproxy reconstruction of paleoceanographic conditions from ODP Site 1168 (Fig. 1b), offshore of western Tasmania, which is located close to the modern position of the subtropical front (STF) and the center of the modern subantarctic–subtropical zone. We reconstruct surface ocean conditions based on dinoflagellate cyst assemblages, a microplankton group that is strongly tied to specific ocean surface conditions: SST, SSS, and nutrients (Thöle et al., 2023). These strict affinities are applied together with previously published biomarker-based sea surface temperature for a detailed reconstruction of changing oceanographic conditions: the latitudinal migration of the subtropical front through time, which potentially deciphers the delayed pCO_2 change with respect to $\delta^{18}O_{bf}$.

2 Materials and methods

2.1 Study site

ODP Site 1168 (42°36.5809′ S, 144°24.7620′ E; 2463 m modern water depth; Fig. 1a) was drilled on the continental slope offshore of western Tasmania (Exon et al., 2001). The Pliocene part of the sequence contains greenish-gray foraminifer-bearing nannofossil ooze with significant detrital clay input (Exon et al., 2001). At present, the STF is located over this site, which separates warm ($> 17\,^{\circ}C$) saline subtropical waters from comparably cold ($< 13\,^{\circ}C$) and fresh subantarctic water masses (Exon et al., 2001; Heath, 1985). Site 1168 is characterized by a modern SST seasonality ranging from 13–17 °C (winter–summer; Reagan et al., 2023) and a modern BWT of 2.5 °C (Exon et al., 2001).

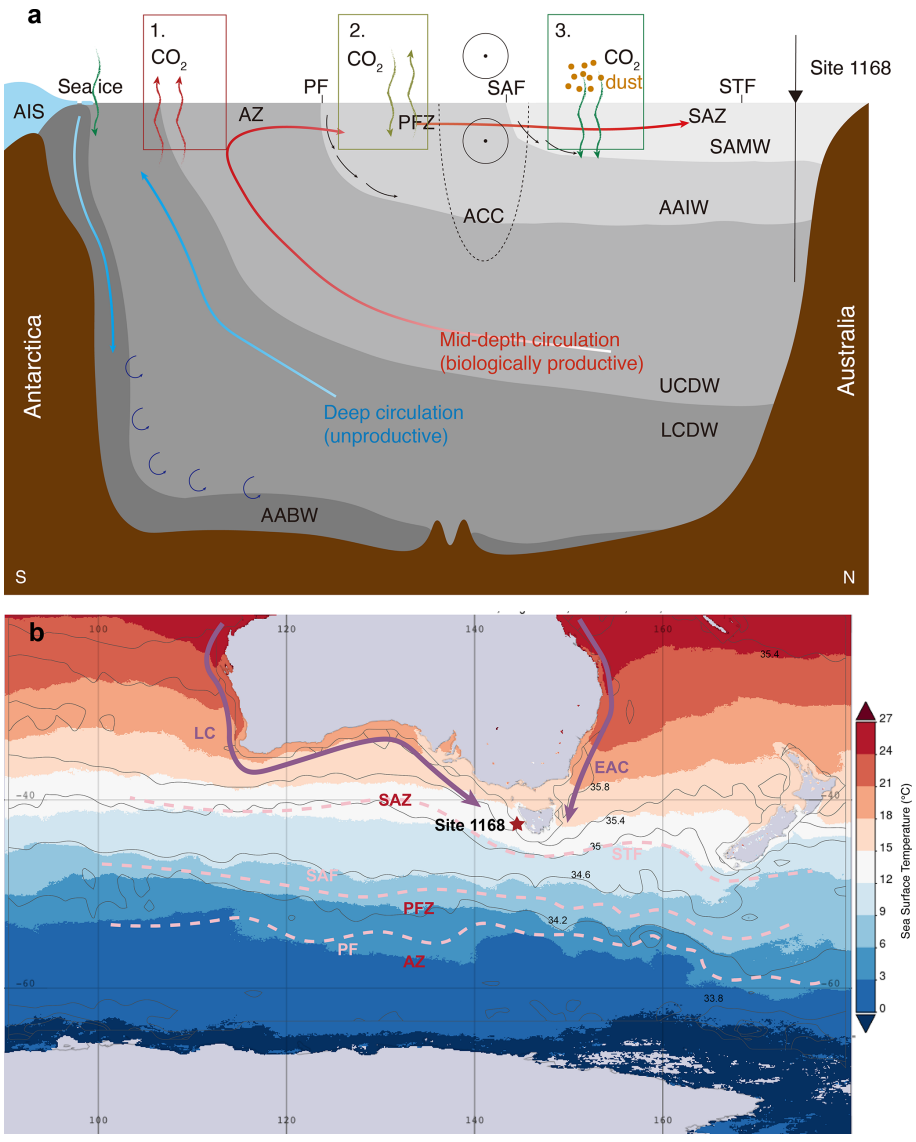

Figure 1. **(a)** Schematic view of the ocean circulation in the Southern Ocean between Antarctica and Australia. Arrows in the ocean denote southern overturning circulation (blue) and mid-depth overturning circulation (red); gray areas depict water masses. SAMW: subantarctic mode water, AAIW: Antarctic Intermediate Water, U/LCDW: Upper/Lower Component Deep Water, AABW: Antarctic Bottom Water, ACC: Antarctic Circumpolar Current. Curvy arrows denote CO_2 uptake or outgassing processes (1. deep-ocean degassing, red; 2. physical diffusion, spring green; 3. biological carbon pump, green). **(b)** Modern location of ODP Site 1168. Colors indicate sea surface temperatures, contours indicate sea surface salinity, and gray blocks indicate the modern coastline and sea ice extent. Purple arrows denote ocean currents (LC: Leeuwin Current, EAC: East Australia Current). Pink dashed lines denote oceanic fronts (STF: subtropical front, SAF: subantarctic front, PF: polar front), and ocean zones in between (SAZ: subtropical–subantarctic zone, PFZ: polar frontal zone, AZ: Antarctic zone) are mentioned in red. Data, maps, and visualizations were generated using the Giovanni online data system (https://giovanni.gsfc.nasa.gov/giovanni/, last access: 1 October 2024) developed and maintained by the National Aeronautics and Space Administration Goddard Earth Sciences Data and Information Services Center (Acker and Leptoukh, 2007). SST and SSS data are derived from the Moderate Resolution Imaging Spectroradiometer on the Aqua satellite (MODIS-Aqua) provided to Giovanni by the Ocean Biology Distributed Active Archive Center.

2.2 Palynology

We processed 56 samples for palynology in the late Pliocene interval. Processing used standard procedures of the GeoLab of Utrecht University (e.g., Brinkhuis et al., 2004). Briefly, this involves first spiking samples with *Lycopodium clavatum* spores prior to palynological processing to allow for quantification of the absolute number of dinocysts per sample (Stockmarr, 1971). Samples were then treated with 30 % hydrochloric acid and ∼ 38 %–40 % hydrofluoric acid to con-

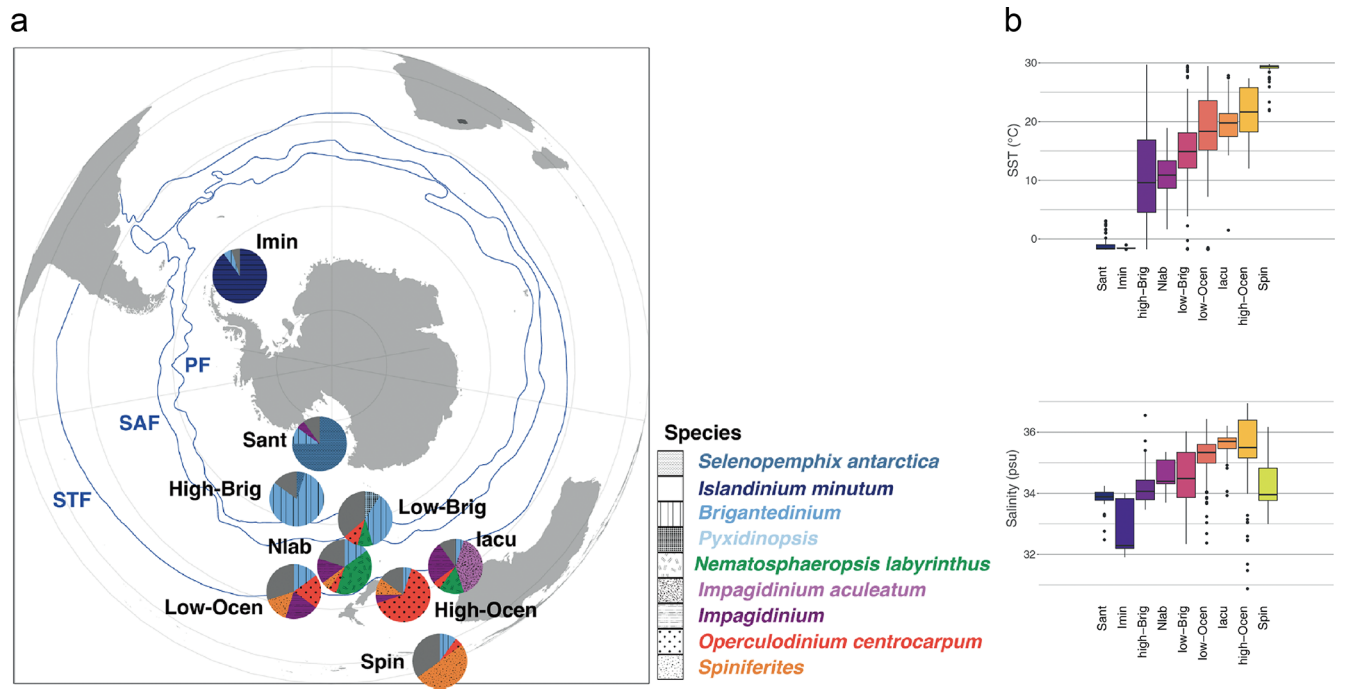

Figure 2. **(a)** Schematic representation of the generalized biogeographic distribution of dinocysts in Southern Ocean surface sediments. Pie charts represent the average assemblage composition of the nine clusters described in this paper. The positions of these pie charts represent their typical latitudinal band of occurrence. Also plotted are the frontal systems (blue lines, STF: subtropical front, SAF: subantarctic front, PF: polar front). The subantarctic zone (SAZ) is the water mass between the STF and PF. **(b)** Comparison of sea surface temperature and sea surface salinity in different clusters for the nine-cluster solution of the modern distribution. The median, 25 %–75 % quantiles, and 95 % confidence interval are indicated by the black line and the boxes and whiskers, respectively. Modified from Thöle et al. (2023).

centrate the acid-resistant organic residue. The isolation of the 10–250 µm fraction was established using nylon mesh sieves and an ultrasonic bath to break up agglutinated particles of the residue. Palynomorphs were counted up to a minimum of 200 identified dinocysts if possible. Taxonomy follows that stated at https://palsys.org (last access: 8 January 2024) (see Bijl and Brinkhuis, 2023). Functional ecological dinocyst groupings follow those derived from modern assemblages (Fig. 2; Thöle et al., 2023). Notably, *Nematosphaeropsis labyrinthus* is characteristic for the Nlab cluster that prevails south of the STF; *Impagidinium aculeatum*, *Operculodinium centrocarpum*, and *Spiniferites* spp. thrive in the Iacu, high-Ocen, and Spin clusters to the north of the STF (Fig. 2). Main taxa are presented in Fig. S2. An STF index is then defined as the relative abundance of dinocyst taxa south of the STF (south of STF/(south + north of STF)) in order to quantitatively demonstrate the migration of the STF, although the index does not directly indicate the latitudinal position of the STF. A higher value of the index indicates that the STF is positioned relatively further north, and vice versa. There are additional dinocyst assemblages specific for Southern Ocean zones further away from the STF (Fig. 2; Thöle et al., 2023). This creates an opportunity to reconstruct past changes in the latitudinal position of the STF through the late Pliocene in detail and, with that, the oceanographic changes in the subantarctic–subtropical carbon sink (see also Hou et al., 2023b). In addition, given that *Impagidinium pallidum*, which is a typical bipolar cold-water species in the modern ocean (the only *Impagidinium* in the ice-proximal Sant cluster; Fig. 2a), seems to have an ambiguous paleo-affinity (De Schepper et al., 2011) and generally low abundance and widespread occurrence in the modern Southern Ocean (Thöle et al., 2023), it is not separated from the other *Impagidinium* in the grouping. Moreover, because the latitudinal position of the STF is representative of the oceanographic fronts associated with the ACC and has implications for the sea ice extent further south, our reconstructions also have implications for the ability of the polar frontal zone to emit CO_2 to the atmosphere.

2.3 Benthic foraminiferal stable isotopes

Each sediment sample was freeze-dried, washed over a 63 µm sieve, oven-dried at 50 °C, and then dry-sieved into different size fractions. We mainly picked tests of *Cibicidoides mundulus* from the 250–355 µm size fraction for our measurements. The picked specimens were cracked between two glass plates, after which the test fragments were ultrasonicated in deionized water (3 × 30 s) to remove adhering sediment, organic lining, and nannofossils. The test fragments

were dried at room temperature overnight. In order to obtain enough material, other benthic species are also processed. We use *Cibicidoides mundulus* and *Cibicidoides (Planulina) wuellerstorfi* for both stable carbon and oxygen.

Stable isotope measurements were performed using a Thermo Scientific MAT 253 Plus and a Thermo Scientific MAT 253 mass spectrometer at the GeoLab of Utrecht University. Both mass spectrometers were coupled to Thermo Fisher Scientific Kiel IV carbonate preparation devices. CO_2 gas was extracted from carbonate samples with phosphoric acid at a reaction temperature of 70 °C. Since both instruments are equipped for clumped isotope analysis, a Porapak trap included in each Kiel IV carbonate preparation system was kept at –40 °C to remove organic contaminants from the sample gas. Between each run, the Porapak trap was heated at 120 °C for at least 1 h for cleaning. Every measurement run included a similar number of samples and three carbonate standards (ETH-1, ETH-2, ETH-3) (Kocken et al., 2019). Two additional reference standards (IAEA-C2 and Merck) were measured in each run to monitor the long-term reproducibility and stability of the instrument. Both the $\delta^{13}C$ and $\delta^{18}O$ values (reported relative to the Vienna Pee Dee Belemnite (VPDB) scale) of IAEA-C2 showed an external reproducibility (standard deviation) of 0.06 ‰.

2.4 Bulk carbonate stable isotopes

Bulk carbonate isotopes were measured as an additional stratigraphic tool alongside the benthic $\delta^{13}C$ and $\delta^{18}O$. For 118 samples, between 50–100 µg of powdered sediment was analyzed on a Thermo Finnigan GasBench II system, coupled to a Thermo Delta V mass spectrometer. Homogenized samples were transferred to sealable vials which were flushed with helium for 5 min per vial to remove atmospheric oxygen and carbon. In each run, 65 samples were then treated with H_3PO_4 at a temperature of 72 °C together with carbonate standards NAXOS (11 times) and IAEA-603 (four times) for the purpose of calibration. All isotope values are reported against VPDB. Analytical precision, as determined by the SD of NAXOS, was better than 0.08 ‰ for $\delta^{18}O$ and 0.04 ‰ for $\delta^{13}C$.

3 Results

3.1 Stable isotopes and age model

The post-expedition age model of sediments from ODP Site 1168 comprises biostratigraphic constraints from nannofossils, foraminifera, diatoms, and dinoflagellate cysts; paleomagnetic constraints; and for the Pleistocene identifications of marine isotope stages from benthic foraminiferal isotopes (Stickley et al., 2004). For the Pliocene–Pleistocene part of the record, the paleomagnetic constraints, which come from Hole B, are structurally offset by around 50 m per 1 million years from biostratigraphic datums and Pleistocene marine isotope stages that come from Hole A, even at splice depth (see Stickley et al., 2004). For a high-resolution age model of the late Pliocene section at Hole A of Site 1168, we generated new benthic foraminiferal and bulk carbonate stable isotope data across the suspected late Pliocene interval from Hole A and compared these to the shipboard color reflectance data (Exon et al., 2001). Cyclicity in both was then compared to orbital cycles seen in the CENOGRID (Westerhold et al., 2020) (Fig. 3). Since all our new data and the stratigraphic constraints except the paleomagnetic reversals derive from Hole A, which yields the longest extent and best recovery, we decided for the purpose of this study to ignore the offset paleomagnetic constraints from Hole B (as published in Stickley et al., 2004, and updated in Hou et al., 2023a) for now and recommend that later studies first revisit the composite depth, stratigraphic correlation, and quality of the magnetic data before including these in the composite age model of the site.

New $\delta^{18}O_{bf}$ and $\delta^{18}O_{bulk}$ between 27–40 m below the sea floor (m b.s.f.) correlate well with color reflectance, whereby low and high $\delta^{18}O$ correlates with high and low lightness of the sediment (Fig. 3). Both show a conspicuous trough at 35.0–35.5 m b.s.f., and based on the available biostratigraphic age model constraints, we interpret that to reflect the MIS M2. Tuning the resulting $\delta^{18}O_{bf}$ and color reflectance record (Exon et al., 2001) to the CENOGRID (Westerhold et al., 2020) resulted in four age tie points (Fig. 3; nos. 3–6), nos. 3 and 4 of which are based on the largest slope, and confidence in the stratigraphic position of MIS M2 isotope excursion. A maximum in $\delta^{18}O_{bulk}$ at 30 m b.s.f. is tuned to MIS G20 (Fig. 3; no. 2) and a minimum at 37 m b.s.f. is tuned to MIS MG3 (Fig. 3; no. 8). Two additional stratigraphic tie points were chosen by tuning the color reflectance record to the CENOGRID stack further up- and down-section (Fig. 3; nos. 1, 7). See Table S1 in the Supplement for the stratigraphic tie points in this paper and the resulting age model. Linear regression indicates a sedimentation rate of 1.88 cm kyr^{-1} (Fig. 4).

3.2 Sea surface temperature

SST records of Pliocene Site 1168 have been previously published (Hou et al., 2023a). SST proxies, $U^{k'}_{37}$ and TEX_{86}, were calculated based on alkenones and glycerol dialkyl glycerol tetraethers (GDGTs), respectively. $U^{k'}_{37}$-based SSTs were determined using core-top linear calibration (Müller et al., 1998). $U^{k'}_{37}$-based SSTs vary around 17 °C prior to MIS M2. They decrease to 12 °C at the peak of the MIS M2 glaciation (Fig. 5a). In the mPWP, SST varies around 14 °C, which is approximately 2 °C lower than the pre-M2 interval (Fig. 5a). Additionally, SST at KM5c yields 14.5 °C.

TEX_{86}-based SSTs are determined by both core-top exponential (TEX^{H}_{86}; Kim et al., 2010) and Bayesian calibration (BAYSPAR; Tierney and Tingley, 2014). In general, TEX_{86}-based SSTs resemble those derived from $U^{k'}_{37}$ in trend; how-

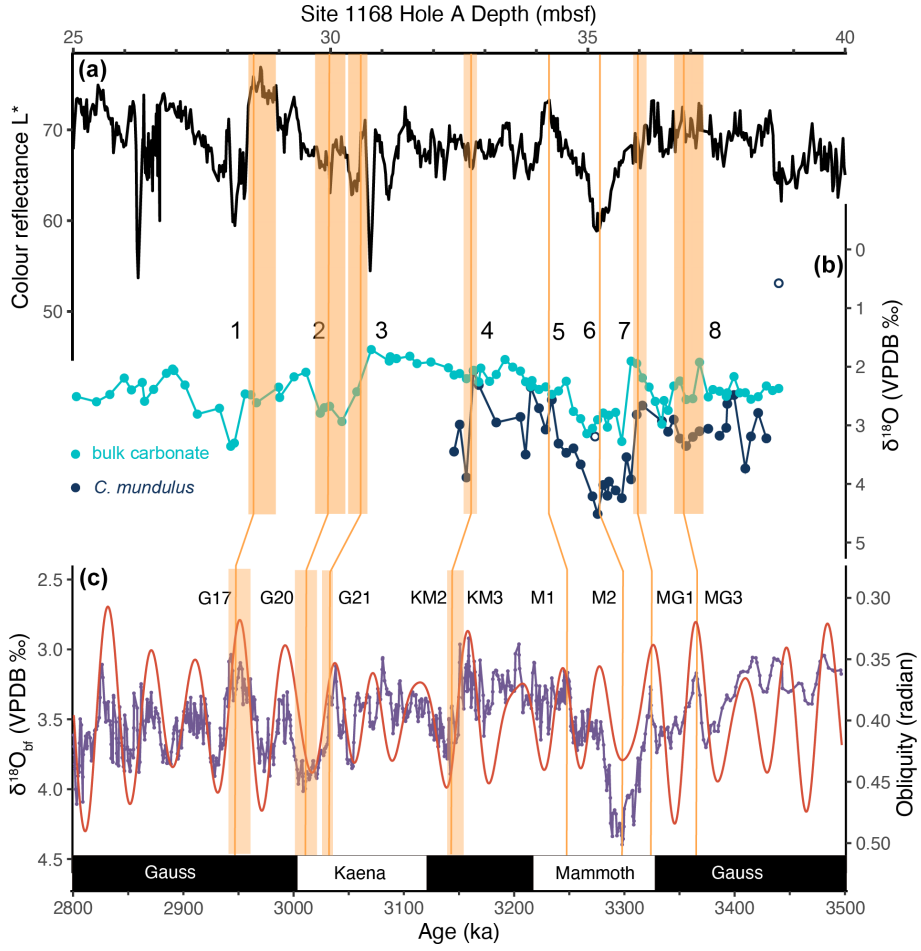

Figure 3. Age tuning for the Pliocene of ODP Site 1168 Hole A. **(a)** L* color reflectance of Site 1168A (Exon et al., 2001). **(b)** $\delta^{18}O_{bf}$ and $\delta^{18}O_{bulk}$ of Site 1168A, **(c)** CENOGRID (Westerhold et al., 2020), and an obliquity insolation curve (Laskar et al., 2004) using the software Acycle (Li et al., 2019). Orange lines indicate tie points, and orange rectangles indicate errors in depth or age.

ever, the amplitude of cooling at MIS M2 is ∼ 3 °C higher, which we cannot ascribe to the confounding factor of the GDGT-2 to GDGT-3 ratio, a general indicator for additional deep-water contributions to TEX_{86} (Taylor et al., 2013; Ho and Laepple, 2016; Van der Weijst et al., 2022), that do not change across the MIS M2 (Hou et al., 2023a).

3.3 Dinocyst assemblage

Pliocene dinocyst assemblages at Site 1168 are broadly similar to modern assemblages around the subtropical front and thus enable us to use information on the modern affinities of these species (Thöle et al., 2023) to reconstruct paleoceanographic conditions at this site. Prior to 3400 ka, the STF index is about 0.3 and assemblages are typical for modern regions north of the STF (Fig. 5b), with abundant *O. centrocarpum* (High-Ocen cluster), *I. aculeatum* (Iacu cluster), and *Spiniferites* spp. (Spin cluster; Thöle et al., 2023). The increase in *N. labyrinthus* (around 3400 ka) makes the assemblages progressively more similar to those of the SAZ, south of the STF, and forms the Nlab cluster when it is dominant in the assemblage (> 40 %). The attendance of *I. pallidum* is sporadic throughout the record; however, it transiently increases to ∼ 10 % at 3300 ka and dominates the other *Impagidinium* group (see raw data). The abundance of *N. labyrinthus* peaks at 3275 ka and the STF index reaches 0.8, well after the peak of MIS M2, in its deglaciation stage (Fig. 5b). Thereafter, assemblages north of STF recovered and replaced *N. labyrinthus* in the mPWP. The total concentration and total burial flux of dinocysts are generally stable throughout the record but culminate 4-fold at 3240 ka (34.05 m b.s.f.; Fig. S1 in the Supplement).

4 Discussion

4.1 STF migrations and SAZ surface conditions in the late Pliocene

The lowest local SSTs (13 °C based on $U^{k'}_{37}$) were recorded at peak MIS M2 glaciation: ∼ 6 °C lower than those before

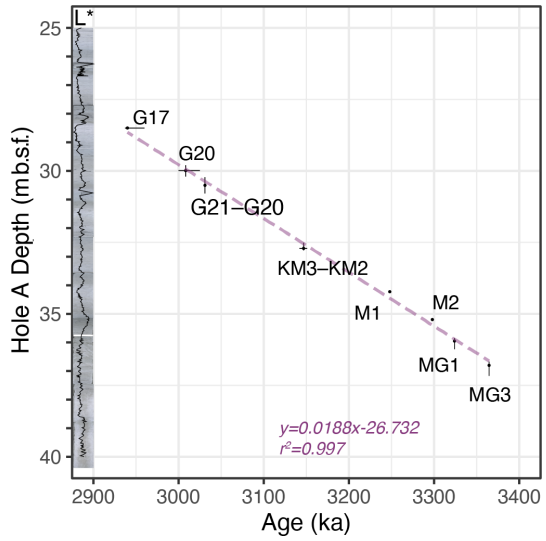

Figure 4. Age–depth plot of Site 1168 Hole A along with core photos (Core3H6W–Core5H3 W) and L* color reflectance in the late Pliocene. Tie points are presented in Fig. 3. Vertical error bars indicate potential errors in depth when tie points are assigned based on $\delta^{18}O_{bf}$ and $\delta^{18}O_{bulk}$; see Table S1. The purple dashed line indicates a linear regression for an estimation of sedimentation rate, which is used for dinocyst burial flux calculation; see the Supplement and Fig. S1.

M2 and ∼ 5 °C lower than those in the mPWP (Fig. 5a). The amplitude of the SST variation over the mPWP glacial–interglacial cycles is about 1–2 °C, much smaller than the cooling associated with M2. In terms of the cooling amplitude, SSTs at low to middle latitudes during MIS M2 suggest an unusually strong glacial (Lawrence et al., 2009; De Schepper et al., 2013; Liu et al., 2019, 2022; Van der Weijst et al., 2022). However, temperature reconstructions from the high-latitude surface (Bachem et al., 2017; Risebrobakken et al., 2016) and deep ocean (Braaten et al., 2023) suggest that either MIS M2 indicates no profound cooling or the cooling has a similar amplitude as other glacial phases within the mPWP. The extreme SST response to MIS M2 in the subantarctic zone is therefore extraordinary and perhaps not the result of radiative forcing but is amplified by regional or local oceanographic changes. Furthermore, SSTs of Site 1168 are highly consistent with the subsurface temperature of Site 959, recording South Atlantic Central Water, which derives from the Southern Hemisphere subtropical surface ocean (SACW; Van der Weijst et al., 2022). Therefore, their similarity to surface temperatures at Site 1168 is not surprising.

The dinocyst assemblage indicates that the most northern position of the STF is reached during the M2–mPWP transition, i.e., when SST at ODP Site 1168 increased over 5 °C (Fig. 5a and b). During both the peak and deglaciation of MIS M2, SSTs at 1168 are within the modern SST range of the Nlab cluster (Fig. 2), although the 15–17 °C (both proxies) at deglaciation does approach the upper limit of the SST range of the Nlab cluster (Fig. 2b; Thöle et al., 2023). Based on the modern dinocyst distributions (Fig. 2b), and in particular the proliferation of *N. labyrinthus* (Fig. 5b), the surface ocean might have become fresher during MIS M2 deglaciation compared to pre-M2 according to their modern affinities (Thöle et al., 2023). Since there is no evidence in the palynological slides or in GDGT-based indices (Hou et al., 2023a) for enhanced terrestrial input from runoff, we infer that the surface ocean freshening of the subantarctic zone at M2 deglaciation originated from excessive iceberg discharge, which eventually melted in the SAZ or the massive iceberg melting would have impacted a larger area than its spatial presence (Merino et al., 2016).

Overall, according to the changes we observed in dinocyst assemblages, we estimate that the STF was positioned to the south of Site 1168 from prior to MIS M2 until its onset; the STF moved northward as SST decreased and *N. labyrinthus* increased during M2. During the deglaciation of MIS M2, the STF moved further northward and approached the margin of Tasmania (42° S) at 3275 ka, and surface waters strongly freshened. During the mPWP, the surface salinity at Site 1168 normalized and the STF shifted poleward to a similar position as before M2 (Fig. 5b).

Our interpretation of the dinocyst assemblage is mainly based on its modern distribution (Thöle et al., 2023). An evolutionary shift in the ecological affinity of a dinocyst assemblage or cluster can influence an absolute quantitative estimation of paleo-oceanic conditions. In light of that, modern analogues of dinocyst distribution should be applied with some degree of caution. For example, *Impagidinium pallidum* is restricted to polar regions in the modern ocean (Zonneveld et al., 2013); however, it thrived at lower latitudes in the Neogene and was associated with higher SSTs (De Schepper et al., 2011; Hennissen et al., 2017). However, the most abundant extant species such as *O. centrocarpum* and *N. labyrinthus* are shown to have comparable SST ranges in the past, by referring to geochemical proxies (De Schepper et al., 2011; Hoem et al., 2021, 2022; Hou et al., 2023b; Sangiorgi et al., 2018), and today. Besides temperature affinities, dinocyst distributions can also indicate salinity in the modern ocean. However, quantitative salinity reconstructions remain scarce, and as a result the absolute range of salinities for the Pliocene is unknown. Thus, we can only postulate relative surface salinity change across MIS M2. Given the dinocyst assemblage record found at Site 1168, an alternation from a warm (*I. aculeatum* and *O. centrocarpum*) to cool (*N. labyrinthus*) assemblage is distinctive, which was similarly discovered in the Pliocene North Atlantic (De Schepper et al., 2009, 2011).

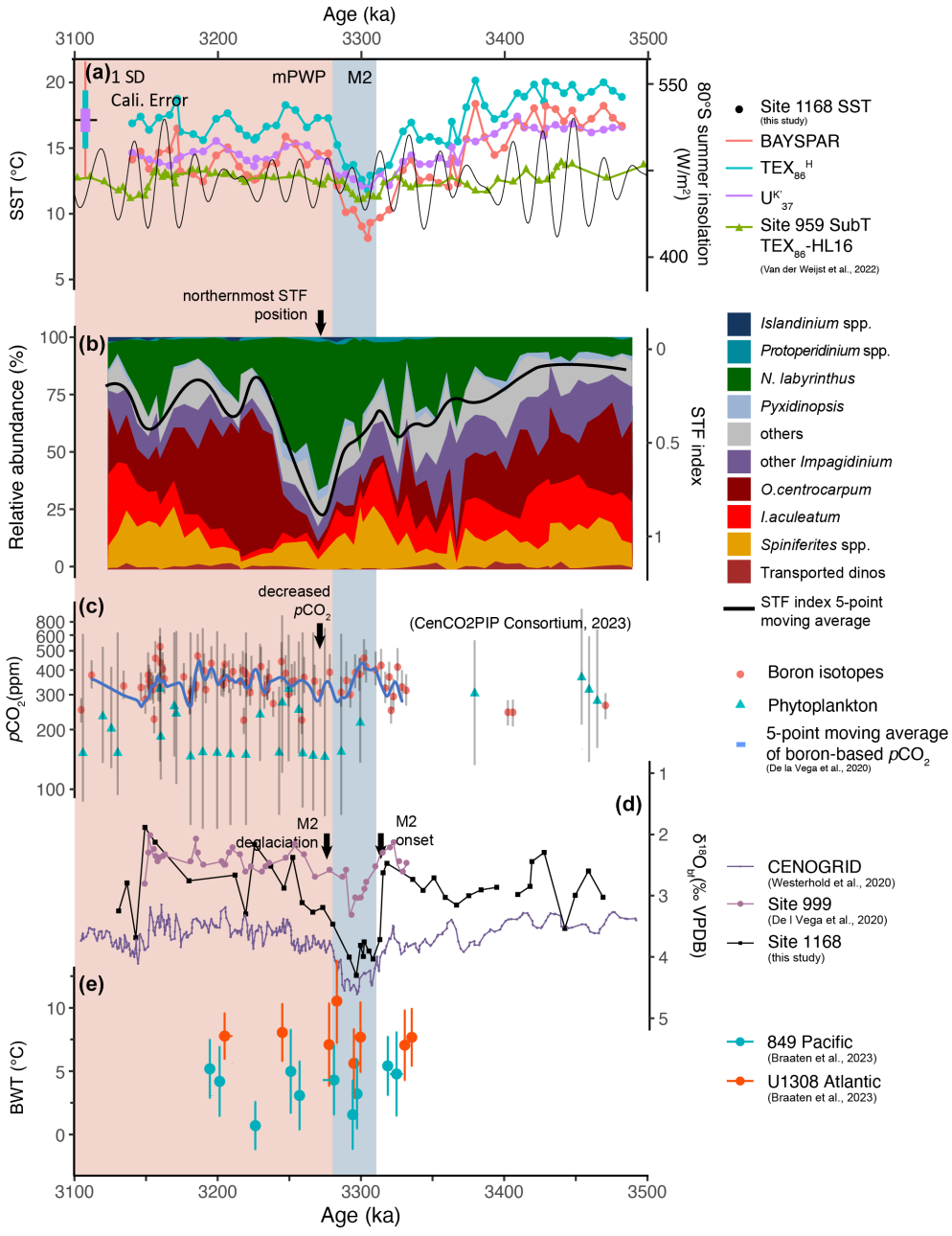

Figure 5. Late Pliocene proxy compilation for oceanographic change at ODP Site 1168 and published pCO_2 and BWT reconstructions. **(a)** Sea surface temperature at Site 1168 based on TEX_{86} (exponential TEX_{86}^{H} and BAYSPAR calibrations; Kim et al., 2010; Tierney and Tingley, 2014) and $U_{37}^{k'}$ (linear calibration; Müller et al., 1998). Subsurface temperature at Site 959 (Van der Weijst et al., 2022) using the HL-16 calibration (Ho and Laepple, 2016). Antarctic summer (80° S, January) insolation on the second y axis (Laskar et al., 2004; De Boer et al., 2014). **(b)** Dinocyst assemblages of Site 1168; green indicates species south of STF; orange, red, and burgundy indicate species north of STF; and blueish-green and blue indicate high-productivity and/or sea-ice-affiliated species (Thöle et al., 2023). The black line represents a five-point moving average of the dinocyst-based STF index (south of STF/(south + north of STF)) roughly indicating the position of the STF at ODP Site 1168 that we derive from these dinocyst assemblages (up or 0 is north, down or 1 is south). **(c)** pCO_2 derived from boron isotopes (red dots) and alkenone $\delta^{13}C$ (cyan triangles) (CenCO2PIP Consortium, 2023, and references therein) as well as a five-point moving average record based on boron isotopes (blue curve); the vertical error bar is the 95 % confidence interval. **(d)** Benthic foraminiferal $\delta^{18}O$ of ODP Site 1168 and Site 999 (De la Vega et al., 2020) as well as the global stack (Westerhold et al., 2020). **(e)** Bottom water temperature of ODP Site 849 (blue dots) and IODP Site U1308 (orange dots, Braaten et al., 2023); the vertical error bar is the 95 % confidence interval, and the horizontal error bar is the averaged age range. The pink rectangle indicates the mid-Piacenzian warm period, and the blue rectangle indicates Marine Isotope Stage M2.

4.2 Southern Ocean carbon outgassing as a pCO_2 regulator across M2

By combining our reconstructed STF migrations with the available pCO_2 reconstructions of the late Pliocene, we note a coincidence that the northernmost position of the STF is likely synchronous with the lowest pCO_2, which are both 10–20 kyr later than MIS M2 (De la Vega et al., 2020). The offset between pCO_2 from Site 999 and the SST and isotope data shown from Site 1168 is age-model-independent. Although $\delta^{18}O$ records of Site 1168 and Site 999 have demonstrated a reliable stratigraphic match (Fig. 5d), uncertainties remain regarding whether the northernmost position of the STF and decreased pCO_2 are really so directly coupled, given the errors in respective age models and the resolution of both records. This leaves room for a small offset between the STF migration and pCO_2 decline but cannot explain the offset between global CO_2 and SST at Site 1168. The bulk of the late Pliocene pCO_2 record is generated from ODP Site 999 (Caribbean Sea), for which the surface air–sea disequilibrium for CO_2 is close to 0 (Martínez-Botí et al., 2015). Because of that, this Caribbean Sea site has been used in multiple studies to reconstruct past global pCO_2 (Chalk et al., 2017; De la Vega et al., 2020, 2023; Foster, 2008).

At the onset of MIS M2, pCO_2 was about 400 ppm (De la Vega et al., 2020) and Site 1168 had an abundance of warm species such as *O. centrocarpum*, *I. aculeatum*, and *Spiniferites* spp. (Thöle et al., 2023), suggesting a southernly position of the STF. Following this maximum, the STF was moving northwards during the MIS M2 $\delta^{18}O$ peak and the coolest SSTs (Fig. 5a). However, The STF reached its northernmost position in the deglaciation phase of the M2 event, and this corresponds to the lowest pCO_2 (Fig. 5c). During the mPWP, when SST was high, the STF migrated back southward and pCO_2 gradually increased to $\sim$ 400 ppm. The decreased SST and probably salinity should have enhanced the oceanic net uptake of atmospheric CO_2 at MIS M2, which had a negative effect on pCO_2; however, it is contradictory to the high pCO_2 reconstructed. Past studies have combined similar dinocyst and SST records across MIS M2 in the North Atlantic, along the path of Atlantic Meridional Overturning Circulation (AMOC; e.g., De Schepper et al., 2009b, 2013, 2014). In those records, no obvious leads or lags can be observed between dinocyst assemblages, SST, and $\delta^{18}O_{bf}$. Such a spatial difference between the North Atlantic (De Schepper et al., 2009, 2013, 2014) and the Southern Ocean (this study) may be accounted for by different forcing processes. Thus, the mechanism we propose involves the ocean as a source and sink of atmospheric CO_2 (Kirby et al., 2020) and the shifting fronts and Antarctic ice extent (Toggweiler et al., 2006) due to the hysteresis of the East Antarctic ice sheet. Our data show that the two subpolar zones behaved fundamentally differently during the MIS M2 deglaciation phase. Our data are compatible with the hypothesis proposed by Toggweiler et al. (2006); however, other modeling studies do show opposite results (Gottschalk et al., 2019, and references therein). It should be noted that some feedback mechanisms associated with westerlies and front shifts are incompletely represented in models; for instance, Antarctic sea ice cover and ice sheet calving (Gottschalk et al., 2019) can seriously impact the outputs. It is noteworthy that the consistency of our results with those of Toggweiler et al. (2006) adds to the debate on how oceanography and atmospheric CO_2 interact.

The migrations of the oceanic fronts including the STF in the Tasmanian sector are the consequences of shifts in the westerlies and Antarctic-proximal sea ice extent – in the Pleistocene and Miocene (Groeneveld et al., 2017; Hou et al., 2023b; Kohfeld and Chase, 2017) but also in the Pliocene. During the M2, the STF gradually shifted northward, indicating an equivalent shift of the westerlies and a northward expansion of the subantarctic zone. The northward migration of the westerlies and fronts enhanced the stratification of the Southern Ocean and thereby prevented respired CO_2 from outgassing into the atmosphere. Consequently, pCO_2 dropped, in phase with the northward migration of the STF. At the same time, the freshening of the surface SAZ (Fig. 1) must have lowered carbon uptake in the surface ocean (Bourgeois et al., 2022). However, the decreased pCO_2 apparently suggests that the lowered surface carbon uptake did not compensate for the reduction of emissions induced by the expanding sea ice cover in the polar frontal zone. The equatorward shift of the STF, which continued into the deglaciation stage of MIS M2, was associated with expanded sea ice cover in the polar frontal zone, especially in the deglaciation stage, when surface waters freshened. The higher amplitude of obliquity increased Antarctic summer insolation after the MIS M2 peak glacial advance (Fig. 5a) and this probably enhanced iceberg calving (De Boer et al., 2014), which stimulated the northward migration and freshening of the STF. Furthermore, Antarctic ice sheet simulations suggest that insolation-driven sub-shelf melting can be linked to changes in the carbon cycle (De Boer et al., 2014). Indeed, massive iceberg calving was noticed at the East Antarctic margin during periods of deglaciation in the Pliocene, associated with maximum iceberg-rafted debris (Cook et al., 2013; Patterson et al., 2014), which is in line with our frontal migration record. Furthermore, geochemical evidence from the North Atlantic excludes the deep Atlantic Ocean as a principle carbon sink, implying a Southern Ocean driving mechanism (Kirby et al., 2020), which is in line with our observations.

When the M2 deglaciation was complete, in the mPWP, iceberg discharge ceased (Patterson et al., 2014) because in the sector of Antarctica nearest to our site fewer glaciers terminated in the ocean (Cook et al., 2013), sea ice cover decreased (Patterson et al., 2014), and westerlies moved southward. As such, shifts in sea ice cover over the polar front controlled air–sea gas exchange: the weaker the sea ice cover, the less stratification and the more CO_2 outgassing from the CO_2-rich deep water. Similar mechanisms, involving sea ice

cover as a regulator for Southern Ocean air–sea CO_2 exchange, have been proposed for the Pleistocene and Quaternary (Kohfeld and Chase, 2017; Sigman et al., 2010). Furthermore, the dinocyst-based, poleward-positioned STF in the mPWP fell in line with simulated weak stratification and enhanced outgassing in the Southern Ocean (Zhang et al., 2013), which resulted in elevated pCO_2. However, new PlioMIP2 models yield contradictory results (Weiffenbach et al., 2023). Simulations on the Southern Ocean are thus highly model-dependent (Weiffenbach et al., 2023; Zhang et al., 2021). In any case, present models are not able to resolve frontal migrations or local effects due to their spatial resolution.

Nevertheless, pCO_2 in the Pleistocene (Bereiter et al., 2015; Yan et al., 2019) does not show lags between surface oceanography and benthic $\delta^{18}O$ changes (Chalk et al., 2017; Lisiecki and Raymo, 2005; Martínez-Garcia et al., 2010) as much as the M2–mPWP interval shows here. Shifts in westerlies further drove variations of dust input to the Pleistocene ocean (Abell et al., 2021) and influenced CO_2 uptake through the biological carbon pump (Thöle et al., 2019). Essentially, its impact on carbon storage was in phase with deep-ocean CO_2 degassing, e.g., inducing lower pCO_2 in the Pleistocene glacial maxima (Ai et al., 2020, 2024; Ziegler et al., 2013). However, late Pliocene aeolian input was limited both regionally in the Southern Ocean (Martínez-Garcia et al., 2010; Naafs et al., 2012) and globally (Teruel et al., 2021), and therefore this process played a less important role during the Pliocene. M2 glaciation occurred mainly as orbitally forced ice buildup and did not seem to have been triggered by a decline in pCO_2 (De la Vega et al., 2020). A new study of Δ_{47}-based BWTs in the North Atlantic and North Pacific has found that deep-sea cooling lags the positive $\delta^{18}O$ excursion of M2 by ~ 20 kyr (Fig. 5d and e; Braaten et al., 2023) but is in phase with the pCO_2 variations (De la Vega et al., 2020). Therefore, moderate changes in Pliocene pCO_2 across the M2 were independent of global ice volume change but instead linked to oceanographic changes (including deep-ocean temperature) through the pCO_2–global climate positive feedback (Braaten et al., 2023).

5 Conclusions

Our new Pliocene dinocyst assemblage data combined with previously published SSTs from the same site shed new light on the dynamics of Southern Ocean frontal systems in relation to ice sheets and sea ice. The reconstructions show that the STF migrated substantially across the M2–mPWP climatic transition. Vast sea ice extent and iceberg discharge during the deglaciation stage of MIS M2 pushed the STF to its northernmost position, freshened it, and prevented respired CO_2 emissions from the deep ocean to the atmosphere. This suggests that, across the MIS M2 event, Southern Ocean frontal migrations controlled ocean–air CO_2 exchange and resulted in the pCO_2 changes on orbital timescales.

Data availability. The new palynological and benthic and bulk stable isotope data from Site 1168 are deposited on Zenodo at https://doi.org/10.5281/zenodo.13850979 (Hou, 2024). All other data presented have been deposited already, and references to those repository items can be found in the respective publications.

Supplement. The supplement related to this article is available online at: https://doi.org/10.5194/cp-21-79-2025-supplement.

Author contributions. PKB designed the research. SH and LT processed and analyzed samples for palynology, and SH and PKB interpreted the palynological results. SH and MvdL washed and picked benthic foraminifera and generated the stable and clumped isotope data. FR measured the bulk carbonate isotopes. SH, LJL, and PKB refined the age model. SH wrote the paper with input from PKB, LJL, and MZ. All authors have contributed to the submitted manuscript.

Competing interests. The contact author has declared that none of the authors has any competing interests.

Disclaimer. Publisher's note: Copernicus Publications remains neutral with regard to jurisdictional claims made in the text, published maps, institutional affiliations, or any other geographical representation in this paper. While Copernicus Publications makes every effort to include appropriate place names, the final responsibility lies with the authors.

Acknowledgements. We thank Mariska Hoorweg, Natasja Welters, Giovanni Dammers, Desmond Eefting, and Arnold van Dijk for laboratory assistance. We thank IODP and scientists of ODP Leg 189, as well as technicians at KCC in Kochi, Japan, for making samples and data available. We are grateful to Lena Thöle, Julia Weiffenbach, Fenghao Liu, and Anna Braaten for discussions and the latter also for providing revised clumped isotope data.

Review statement. This paper was edited by Bjørg Risebrobakken and reviewed by Jan Hennissen and one anonymous referee.

Financial support. This research has been supported by the H2020 European Research Council (OceaNice (grant no. 802835)).

References

Abell, J. T., Winckler, G., Anderson, R. F., and Herbert, T. D.: Poleward and weakened westerlies during Pliocene warmth, Nature, 589, 70–75, https://doi.org/10.1038/s41586-020-03062-1, 2021.

Acker, J. G. and Leptoukh, G.: Online analysis enhances use of NASA Earth science data, Eos T. Am. Geophys. Un., 88, 14–17, https://doi.org/10.1029/2007EO020003, 2007.

Ai, X. E., Studer, A. S., Sigman, D. M., Martínez-García, A., Fripiat, F., Thöle, L. M., Michel, E., Gottschalk, J., Arnold, L., Moretti, S., Schmitt, M., Oleynik, S., Jaccard, S. L., and Haug, G. H.: Southern Ocean upwelling, Earth's obliquity, and glacial-interglacial atmospheric CO_2 change, Science, 370, 1348–1352, https://doi.org/10.1126/science.abd2115, 2020.

Ai, X. E., Thöle, L. M., Auderset, A., Schmitt, M., Moretti, S., Studer, A. S., Michel, E., Wegmann, M., Mazaud, A., Bijl, P. K., Sigman, D. M., Martínez-García, A., and Jaccard, S. L.: The southward migration of the Antarctic Circumpolar Current enhanced oceanic degassing of carbon dioxide during the last two deglaciations, Commun. Earth Environ., 5, 1–12, https://doi.org/10.1038/s43247-024-01216-x, 2024.

Bachem, P. E., Risebrobakken, B., De Schepper, S., and McClymont, E. L.: Highly variable Pliocene sea surface conditions in the Norwegian Sea, Clim. Past, 13, 1153–1168, https://doi.org/10.5194/cp-13-1153-2017, 2017.

Bereiter, B., Eggleston, S., Schmitt, J., Nehrbass-Ahles, C., Stocker, T. F., Fischer, H., Kipfstuhl, S., and Chappellaz, J.: Revision of the EPICA Dome C CO_2 record from 800 to 600 kyr before present, Geophys. Res. Lett., 42, 542–549, https://doi.org/10.1002/2014GL061957, 2015.

Bijl, P. K. and Brinkhuis, H.: Palsys.org: an open-access taxonomic and stratigraphic database of organic-walled dinoflagellate cysts, J. Micropalaeontol., 42, 309–314, https://doi.org/10.5194/jm-42-309-2023, 2023.

Bourgeois, T., Goris, N., Schwinger, J., and Tjiputra, J. F.: Stratification constrains future heat and carbon uptake in the Southern Ocean between 30° S and 55° S, Nat. Commun., 13, 340, https://doi.org/10.1038/s41467-022-27979-5, 2022.

Braaten, A. H., Jakob, K. A., Ho, S. L., Friedrich, O., Galaasen, E. V., De Schepper, S., Wilson, P. A., and Meckler, A. N.: Limited exchange between the deep Pacific and Atlantic oceans during the warm mid-Pliocene and Marine Isotope Stage M2 "glaciation", Clim. Past, 19, 2109–2125, https://doi.org/10.5194/cp-19-2109-2023, 2023.

Brinkhuis, H., Munsterman, D. K., Sengers, M. J., Sluijs, A., Warnaar, J., and Williams, G. L.: Late eocene – Quaternary dinoflagellate cysts from odp site1168, Off Western Tasmania, Ocean Drilling Program, https://doi.org/10.2973/odp.proc.sr.189.2004, 2004.

Burton, L. E., Haywood, A. M., Tindall, J. C., Dolan, A. M., Hill, D. J., Abe-Ouchi, A., Chan, W.-L., Chandan, D., Feng, R., Hunter, S. J., Li, X., Peltier, W. R., Tan, N., Stepanek, C., and Zhang, Z.: On the climatic influence of CO_2 forcing in the Pliocene, Clim. Past, 19, 747–764, https://doi.org/10.5194/cp-19-747-2023, 2023.

CenCO2PIP Consortium: Toward a Cenozoic history of atmospheric CO_2, Science, 382, eadi5177, https://doi.org/10.1126/science.adi5177, 2023.

Chalk, T. B., Hain, M. P., Foster, G. L., Rohling, E. J., Sexton, P. F., Badger, M. P. S., Cherry, S. G., Hasenfratz, A. P., Haug, G. H., Jaccard, S. L., Martínez-García, A., Pälike, H., Pancost, R. D., and Wilson, P. A.: Causes of ice age intensification across the Mid-Pleistocene Transition, P. Natl. Acad. Sci. USA, 114, 13114–13119, https://doi.org/10.1073/pnas.1702143114, 2017.

Cook, C. P., van de Flierdt, T., Williams, T., Hemming, S. R., Iwai, M., Kobayashi, M., Jimenez-Espejo, F. J., Escutia, C., González, J. J., Khim, B.-K., McKay, R. M., Passchier, S., Bohaty, S. M., Riesselman, C. R., Tauxe, L., Sugisaki, S., Galindo, A. L., Patterson, M. O., Sangiorgi, F., Pierce, E. L., Brinkhuis, H., Klaus, A., Fehr, A., Bendle, J. A. P., Bijl, P. K., Carr, S. A., Dunbar, R. B., Flores, J. A., Hayden, T. G., Katsuki, K., Kong, G. S., Nakai, M., Olney, M. P., Pekar, S. F., Pross, J., Röhl, U., Sakai, T., Shrivastava, P. K., Stickley, C. E., Tuo, S., Welsh, K., and Yamane, M.: Dynamic behaviour of the East Antarctic ice sheet during Pliocene warmth, Nat. Geosci., 6, 765–769, https://doi.org/10.1038/ngeo1889, 2013.

De Boer, B., Lourens, L. J., and van de Wal, R. S. W.: Persistent 400 000 year variability of Antarctic ice volume and the carbon cycle is revealed throughout the Plio-Pleistocene, Nat. Commun., 5, 2999, https://doi.org/10.1038/ncomms3999, 2014.

De la Vega, E., Chalk, T. B., Wilson, P. A., Bysani, R. P., and Foster, G. L.: Atmospheric CO_2 during the Mid-Piacenzian Warm Period and the M2 glaciation, Sci. Rep., 10, 11002, https://doi.org/10.1038/s41598-020-67154-8, 2020.

De la Vega, E., Chalk, T. B., Hain, M. P., Wilding, M. R., Casey, D., Gledhill, R., Luo, C., Wilson, P. A., and Foster, G. L.: Orbital CO_2 reconstruction using boron isotopes during the late Pleistocene, an assessment of accuracy, Clim. Past, 19, 2493–2510, https://doi.org/10.5194/cp-19-2493-2023, 2023.

De Schepper, S., Head, M. J., and Groeneveld, J.: North Atlantic Current variability through marine isotope stage M2 (circa 3.3 Ma) during the mid-Pliocene, Paleoceanography, 24, https://doi.org/10.1029/2008PA001725, 2009.

De Schepper, S., Fischer, E. I., Groeneveld, J., Head, M. J., and Matthiessen, J.: Deciphering the palaeoecology of Late Pliocene and Early Pleistocene dinoflagellate cysts, Palaeogeogr. Palaeocl., 309, 17–32, https://doi.org/10.1016/j.palaeo.2011.04.020, 2011.

De Schepper, S., Groeneveld, J., Naafs, B. D. A., Van Renterghem, C., Hennissen, J., Head, M. J., Louwye, S., and Fabian, K.: Northern Hemisphere Glaciation during the Globally Warm Early Late Pliocene, PLoS ONE, 8, e81508, https://doi.org/10.1371/journal.pone.0081508, 2013.

De Schepper, S., Gibbard, P. L., Salzmann, U., and Ehlers, J.: A global synthesis of the marine and terrestrial evidence for glaciation during the Pliocene Epoch, Earth-Sci. Rev., 135, 83–102, https://doi.org/10.1016/j.earscirev.2014.04.003, 2014.

Egleston, E. S., Sabine, C. L., and Morel, F. M. M.: Revelle revisited: Buffer factors that quantify the response of ocean chemistry to changes in DIC and alkalinity, Global Biogeochem. Cy., 24, GB1002, https://doi.org/10.1029/2008GB003407, 2010.

Exon, N. F., Kennett, J. P., and Malone, M. J.: Ocean Drilling Program Leg 189 Initial Reports, Chap. 3, http://www-odp.tamu.edu/publications/189_IR/chap_03/chap_03.htm (last access: 6 January 2025), 2001.

Flesche Kleiven, H., Jansen, E., Fronval, T., and Smith, T. M.: Intensification of Northern Hemisphere glaciations in the circum At-

lantic region (3.5–2.4 Ma) – ice-rafted detritus evidence, Palaeogeogr. Palaeocl., 184, 213–223, https://doi.org/10.1016/S0031-0182(01)00407-2, 2002.

Foster, G. L.: Seawater pH, pCO_2 and [CO2-3] variations in the Caribbean Sea over the last 130 kyr: A boron isotope and B/Ca study of planktic foraminifera, Earth Planet. Sc. Lett., 271, 254–266, https://doi.org/10.1016/j.epsl.2008.04.015, 2008.

Friedlingstein, P., O'Sullivan, M., Jones, M. W., Andrew, R. M., Gregor, L., Hauck, J., Le Quéré, C., Luijkx, I. T., Olsen, A., Peters, G. P., Peters, W., Pongratz, J., Schwingshackl, C., Sitch, S., Canadell, J. G., Ciais, P., Jackson, R. B., Alin, S. R., Alkama, R., Arneth, A., Arora, V. K., Bates, N. R., Becker, M., Bellouin, N., Bittig, H. C., Bopp, L., Chevallier, F., Chini, L. P., Cronin, M., Evans, W., Falk, S., Feely, R. A., Gasser, T., Gehlen, M., Gkritzalis, T., Gloege, L., Grassi, G., Gruber, N., Gürses, Ö., Harris, I., Hefner, M., Houghton, R. A., Hurtt, G. C., Iida, Y., Ilyina, T., Jain, A. K., Jersild, A., Kadono, K., Kato, E., Kennedy, D., Klein Goldewijk, K., Knauer, J., Korsbakken, J. I., Landschützer, P., Lefèvre, N., Lindsay, K., Liu, J., Liu, Z., Marland, G., Mayot, N., McGrath, M. J., Metzl, N., Monacci, N. M., Munro, D. R., Nakaoka, S.-I., Niwa, Y., O'Brien, K., Ono, T., Palmer, P. I., Pan, N., Pierrot, D., Pocock, K., Poulter, B., Resplandy, L., Robertson, E., Rödenbeck, C., Rodriguez, C., Rosan, T. M., Schwinger, J., Séférian, R., Shutler, J. D., Skjelvan, I., Steinhoff, T., Sun, Q., Sutton, A. J., Sweeney, C., Takao, S., Tanhua, T., Tans, P. P., Tian, X., Tian, H., Tilbrook, B., Tsujino, H., Tubiello, F., van der Werf, G. R., Walker, A. P., Wanninkhof, R., Whitehead, C., Willstrand Wranne, A., Wright, R., Yuan, W., Yue, C., Yue, X., Zaehle, S., Zeng, J., and Zheng, B.: Global Carbon Budget 2022, Earth Syst. Sci. Data, 14, 4811–4900, https://doi.org/10.5194/essd-14-4811-2022, 2022.

Gottschalk, J., Battaglia, G., Fischer, H., Frölicher, T. L., Jaccard, S. L., Jeltsch-Thömmes, A., Joos, F., Köhler, P., Meissner, K. J., Menviel, L., Nehrbass-Ahles, C., Schmitt, J., Schmittner, A., Skinner, L. C., and Stocker, T. F.: Mechanisms of millennial-scale atmospheric CO_2 change in numerical model simulations, Quaternary Sci. Rev., 220, 30–74, https://doi.org/10.1016/j.quascirev.2019.05.013, 2019.

Groeneveld, J., Henderiks, J., Renema, W., McHugh, C. M., De Vleeschouwer, D., Christensen, B. A., Fulthorpe, C. S., Reuning, L., Gallagher, S. J., Bogus, K., Auer, G., Ishiwa, T., and Expedition 356 Scientists: Australian shelf sediments reveal shifts in Miocene Southern Hemisphere westerlies, Sci. Adv., 3, e1602567, https://doi.org/10.1126/sciadv.1602567, 2017.

Gruber, N., Gloor, M., Mikaloff Fletcher, S. E., Doney, S. C., Dutkiewicz, S., Follows, M. J., Gerber, M., Jacobson, A. R., Joos, F., Lindsay, K., Menemenlis, D., Mouchet, A., Müller, S. A., Sarmiento, J. L., and Takahashi, T.: Oceanic sources, sinks, and transport of atmospheric CO_2, Global Biogeochem. Cy., 23, GB1005, https://doi.org/10.1029/2008GB003349, 2009.

Gruber, N., Bakker, D. C. E., DeVries, T., Gregor, L., Hauck, J., Landschützer, P., McKinley, G. A., and Müller, J. D.: Trends and variability in the ocean carbon sink, Nat. Rev. Earth Environ., 4, 119–134, https://doi.org/10.1038/s43017-022-00381-x, 2023.

Han, Z., Zhang, Q., Li, Q., Feng, R., Haywood, A. M., Tindall, J. C., Hunter, S. J., Otto-Bliesner, B. L., Brady, E. C., Rosenbloom, N., Zhang, Z., Li, X., Guo, C., Nisancioglu, K. H., Stepanek, C., Lohmann, G., Sohl, L. E., Chandler, M. A., Tan, N., Ramstein, G., Baatsen, M. L. J., von der Heydt, A. S., Chandan, D., Peltier, W. R., Williams, C. J. R., Lunt, D. J., Cheng, J., Wen, Q., and Burls, N. J.: Evaluating the large-scale hydrological cycle response within the Pliocene Model Intercomparison Project Phase 2 (PlioMIP2) ensemble, Clim. Past, 17, 2537–2558, https://doi.org/10.5194/cp-17-2537-2021, 2021.

Haywood, A. M., Tindall, J. C., Dowsett, H. J., Dolan, A. M., Foley, K. M., Hunter, S. J., Hill, D. J., Chan, W.-L., Abe-Ouchi, A., Stepanek, C., Lohmann, G., Chandan, D., Peltier, W. R., Tan, N., Contoux, C., Ramstein, G., Li, X., Zhang, Z., Guo, C., Nisancioglu, K. H., Zhang, Q., Li, Q., Kamae, Y., Chandler, M. A., Sohl, L. E., Otto-Bliesner, B. L., Feng, R., Brady, E. C., von der Heydt, A. S., Baatsen, M. L. J., and Lunt, D. J.: The Pliocene Model Intercomparison Project Phase 2: large-scale climate features and climate sensitivity, Clim. Past, 16, 2095–2123, https://doi.org/10.5194/cp-16-2095-2020, 2020.

Heath, R. A.: A review of the physical oceanography of the seas around New Zealand – 1982, New Zeal. J. Mar. Fresh., 19, 79–124, https://doi.org/10.1080/00288330.1985.9516077, 1985.

Hennissen, J. A. I., Head, M. J., De Schepper, S., and Groeneveld, J.: Dinoflagellate cyst paleoecology during the Pliocene–Pleistocene climatic transition in the North Atlantic, Palaeogeogr. Palaeocl., 470, 81–108, https://doi.org/10.1016/j.palaeo.2016.12.023, 2017.

Ho, S. L. and Laepple, T.: Flat meridional temperature gradient in the early Eocene in the subsurface rather than surface ocean, Nat. Geosci., 9, 606–610, https://doi.org/10.1038/ngeo2763, 2016.

Hoem, F. S., Sauermilch, I., Hou, S., Brinkhuis, H., Sangiorgi, F., and Bijl, P. K.: Late Eocene–early Miocene evolution of the southern Australian subtropical front: a marine palynological approach, J. Micropalaeontol., 40, 175–193, https://doi.org/10.5194/jm-40-175-2021, 2021.

Hoem, F. S., Sauermilch, I., Aleksinski, A. K., Huber, M., Peterse, F., Sangiorgi, F., and Bijl, P. K.: Strength and variability of the Oligocene Southern Ocean surface temperature gradient, Commun. Earth Environ., 3, 322, https://doi.org/10.1038/s43247-022-00666-5, 2022.

Hou, S.: Data from manuscripts "Reconciling equatorward migration of Southern Ocean fronts with minor Antarctic ice volume change during Miocene cooling" and "Southern Ocean control on atmospheric CO_2 changes across late-Pliocene Marine Isotope Stage M2" by Suning Hou and others, Zenodo [data set], https://doi.org/10.5281/zenodo.13850979, 2024.

Hou, S., Lamprou, F., Hoem, F. S., Hadju, M. R. N., Sangiorgi, F., Peterse, F., and Bijl, P. K.: Lipid-biomarker-based sea surface temperature record offshore Tasmania over the last 23 million years, Clim. Past, 19, 787–802, https://doi.org/10.5194/cp-19-787-2023, 2023a.

Hou, S., Stap, L. B., Paul, R., Nelissen, M., Hoem, F. S., Ziegler, M., Sluijs, A., Sangiorgi, F., and Bijl, P. K.: Reconciling Southern Ocean fronts equatorward migration with minor Antarctic ice volume change during Miocene cooling, Nat. Commun., 14, 7230, https://doi.org/10.1038/s41467-023-43106-4, 2023b.

IPCC: Special Report on the Ocean and Cryosphere in a Changing Climate, https://www.ipcc.ch/srocc/ (last access: 6 January 2025), 2019.

Keigwin, L.: Pliocene stable-isotope record of deep sea drilling project site 606: Sequential events of ^{18}O enrichment be-

ginning AT 3.1 MA, U. S. Government Printing Office, https://doi.org/10.2973/dsdp.proc.94.1987, 1987.

Kim, J.-H., van der Meer, J., Schouten, S., Helmke, P., Willmott, V., Sangiorgi, F., Koç, N., Hopmans, E. C., and Damsté, J. S. S.: New indices and calibrations derived from the distribution of crenarchaeal isoprenoid tetraether lipids: Implications for past sea surface temperature reconstructions, Geochim. Cosmochim. Ac., 74, 4639–4654, https://doi.org/10.1016/j.gca.2010.05.027, 2010.

Kirby, N., Bailey, I., Lang, D. C., Brombacher, A., Chalk, T. B., Parker, R. L., Crocker, A. J., Taylor, V. E., Milton, J. A., Foster, G. L., Raymo, M. E., Kroon, D., Bell, D. B., and Wilson, P. A.: On climate and abyssal circulation in the Atlantic Ocean during late Pliocene marine isotope stage M2, ∼ 3.3 million years ago, Quaternary Sci. Rev., 250, 106644, https://doi.org/10.1016/j.quascirev.2020.106644, 2020.

Kocken, I. J., Müller, I. A., and Ziegler, M.: Optimizing the Use of Carbonate Standards to Minimize Uncertainties in Clumped Isotope Data, Geochem. Geophy. Geosy., 20, 5565–5577, https://doi.org/10.1029/2019GC008545, 2019.

Kohfeld, K. E. and Chase, Z.: Temporal evolution of mechanisms controlling ocean carbon uptake during the last glacial cycle, Earth Planet. Sc. Lett., 472, 206–215, https://doi.org/10.1016/j.epsl.2017.05.015, 2017.

Laskar, J., Robutel, P., Joutel, F., Gastineau, M., Correia, A. C. M., and Levrard, B.: A long-term numerical solution for the insolation quantities of the Earth, Aatron. Astrophys., 428, 261–285, https://doi.org/10.1051/0004-6361:20041335, 2004.

Lawrence, K. T., Herbert, T. D., Brown, C. M., Raymo, M. E., and Haywood, A. M.: High-amplitude variations in North Atlantic sea surface temperature during the early Pliocene warm period, Paleoceanography, 24, PA2218, https://doi.org/10.1029/2008PA001669, 2009.

Li, M., Hinnov, L., and Kump, L.: Acycle: Time-series analysis software for paleoclimate research and education, Comput. Geosci., 127, 12–22, https://doi.org/10.1016/j.cageo.2019.02.011, 2019.

Lisiecki, L. E. and Raymo, M. E.: A Pliocene–Pleistocene stack of 57 globally distributed benthic $\delta^{18}O$ records: Pliocene–Pleistocene benthic stack, Paleoceanography, 20, PA1003, https://doi.org/10.1029/2004PA001071, 2005.

Liu, J., Tian, J., Liu, Z., Herbert, T. D., Fedorov, A. V., and Lyle, M.: Eastern equatorial Pacific cold tongue evolution since the late Miocene linked to extratropical climate, Sci. Adv., 5, eaau6060, https://doi.org/10.1126/sciadv.aau6060, 2019.

Liu, X., Huber, M., Foster, G. L., Dessler, A., and Zhang, Y. G.: Persistent high latitude amplification of the Pacific Ocean over the past 10 million years, Nat. Commun., 13, 7310, https://doi.org/10.1038/s41467-022-35011-z, 2022.

Martin, J. H.: Glacial-interglacial CO_2 change: The Iron Hypothesis, Paleoceanography, 5, 1–13, https://doi.org/10.1029/PA005i001p00001, 1990.

Martínez-Botí, M. A., Foster, G. L., Chalk, T. B., Rohling, E. J., Sexton, P. F., Lunt, D. J., Pancost, R. D., Badger, M. P. S., and Schmidt, D. N.: Plio-Pleistocene climate sensitivity evaluated using high-resolution CO_2 records, Nature, 518, 49–54, https://doi.org/10.1038/nature14145, 2015.

Martínez-Garcia, A., Rosell-Melé, A., McClymont, E. L., Gersonde, R., and Haug, G. H.: Subpolar Link to the Emergence of the Modern Equatorial Pacific Cold Tongue, Science, 328, 1550–1553, https://doi.org/10.1126/science.1184480, 2010.

Martínez-García, A., Sigman, D. M., Ren, H., Anderson, R. F., Straub, M., Hodell, D. A., Jaccard, S. L., Eglinton, T. I., and Haug, G. H.: Iron Fertilization of the Subantarctic Ocean During the Last Ice Age, Science, 343, 1347–1350, https://doi.org/10.1126/science.1246848, 2014.

Mas e Braga, M., Jones, R. S., Bernales, J., Andersen, J. L., Fredin, O., Morlighem, M., Koester, A. J., Lifton, N. A., Harbor, J. M., Suganuma, Y., Glasser, N. F., Rogozhina, I., and Stroeven, A. P.: A thicker Antarctic ice stream during the mid-Pliocene warm period, Commun. Earth Environ., 4, 1–13, https://doi.org/10.1038/s43247-023-00983-3, 2023.

McClymont, E. L., Ford, H. L., Ho, S. L., Tindall, J. C., Haywood, A. M., Alonso-Garcia, M., Bailey, I., Berke, M. A., Littler, K., Patterson, M. O., Petrick, B., Peterse, F., Ravelo, A. C., Risebrobakken, B., De Schepper, S., Swann, G. E. A., Thirumalai, K., Tierney, J. E., van der Weijst, C., White, S., Abe-Ouchi, A., Baatsen, M. L. J., Brady, E. C., Chan, W.-L., Chandan, D., Feng, R., Guo, C., von der Heydt, A. S., Hunter, S., Li, X., Lohmann, G., Nisancioglu, K. H., Otto-Bliesner, B. L., Peltier, W. R., Stepanek, C., and Zhang, Z.: Lessons from a high−CO_2 world: an ocean view from ∼ 3 million years ago, Clim. Past, 16, 1599–1615, https://doi.org/10.5194/cp-16-1599-2020, 2020.

McKay, R., Naish, T., Carter, L., Riesselman, C., Dunbar, R., Sjunneskog, C., Winter, D., Sangiorgi, F., Warren, C., Pagani, M., Schouten, S., Willmott, V., Levy, R., DeConto, R., and Powell, R. D.: Antarctic and Southern Ocean influences on Late Pliocene global cooling, P. Natl. Acad. Sci. USA, 109, 6423–6428, https://doi.org/10.1073/pnas.1112248109, 2012.

Merino, N., Le Sommer, J., Durand, G., Jourdain, N. C., Madec, G., Mathiot, P., and Tournadre, J.: Antarctic icebergs melt over the Southern Ocean: Climatology and impact on sea ice, Ocean Model., 104, 99–110, https://doi.org/10.1016/j.ocemod.2016.05.001, 2016.

Müller, P. J., Kirst, G., Ruhland, G., von Storch, I., and Rosell-Melé, A.: Calibration of the alkenone paleotemperature index U37K' based on core-tops from the eastern South Atlantic and the global ocean (60° N–60° S), Geochim. Cosmochim. Ac., 62, 1757–1772, https://doi.org/10.1016/S0016-7037(98)00097-0, 1998.

Naafs, B. D. A., Hefter, J., Acton, G., Haug, G. H., Martínez-Garcia, A., Pancost, R., and Stein, R.: Strengthening of North American dust sources during the late Pliocene (2.7 Ma), Earth Planet. Sc. Lett., 317–318, 8–19, https://doi.org/10.1016/j.epsl.2011.11.026, 2012.

Patterson, M. O., McKay, R., Naish, T., Escutia, C., Jimenez-Espejo, F. J., Raymo, M. E., Meyers, S. R., Tauxe, L., and Brinkhuis, H.: Orbital forcing of the East Antarctic ice sheet during the Pliocene and Early Pleistocene, Nat. Geosci., 7, 841–847, https://doi.org/10.1038/ngeo2273, 2014.

Rae, J. W. B., Burke, A., Robinson, L. F., Adkins, J. F., Chen, T., Cole, C., Greenop, R., Li, T., Littley, E. F. M., Nita, D. C., Stewart, J. A., and Taylor, B. J.: CO_2 storage and release in the deep Southern Ocean on millennial to centennial timescales, Nature, 562, 569–573, https://doi.org/10.1038/s41586-018-0614-0, 2018.

Reagan, J. R., P., B., Tim, E, G., Hernán, A, L., Ricardo, K., B., Olga, Courtney, B., L., C., Scott, V, M., Alexey, R, P., Christopher, Dan, S., Zhankun, W., and Dmitry, D.:

World Ocean Atlas 2023 (NCEI Accession 0270533), NCEI, https://doi.org/10.25921/va26-hv25, 2023.

Risebrobakken, B., Andersson, C., De Schepper, S., and McClymont, E. L.: Low-frequency Pliocene climate variability in the eastern Nordic Seas, Paleoceanography, 31, 1154–1175, https://doi.org/10.1002/2015PA002918, 2016.

Sabine, C. L., Feely, R. A., Gruber, N., Key, R. M., Lee, K., Bullister, J. L., Wanninkhof, R., Wong, C. S., Wallace, D. W. R., Tilbrook, B., Millero, F. J., Peng, T.-H., Kozyr, A., Ono, T., and Rios, A. F.: The Oceanic Sink for Anthropogenic CO_2, Science, 305, 367–371, https://doi.org/10.1126/science.1097403, 2004.

Sangiorgi, F., Bijl, P. K., Passchier, S., Salzmann, U., Schouten, S., McKay, R., Cody, R. D., Pross, J., van de Flierdt, T., Bohaty, S. M., Levy, R., Williams, T., Escutia, C., and Brinkhuis, H.: Southern Ocean warming and Wilkes Land ice sheet retreat during the mid-Miocene, Nat. Commun., 9, 317, https://doi.org/10.1038/s41467-017-02609-7, 2018.

Seki, O., Foster, G. L., Schmidt, D. N., Mackensen, A., Kawamura, K., and Pancost, R. D.: Alkenone and boron-based Pliocene pCO_2 records, Earth Planet. Sc. Lett., 292, 201–211, https://doi.org/10.1016/j.epsl.2010.01.037, 2010.

Shackleton, N. J., Hall, M. A., and Pate: Proceedings of the Ocean Drilling Program, 138 Scientific Results, Ocean Drilling Program, https://doi.org/10.2973/odp.proc.sr.138.1995, 1995.

Sigman, D. M., Hain, M. P., and Haug, G. H.: The polar ocean and glacial cycles in atmospheric CO_2 concentration, Nature, 466, 47–55, https://doi.org/10.1038/nature09149, 2010.

Skinner, L. C., Fallon, S., Waelbroeck, C., Michel, E., and Barker, S.: Ventilation of the Deep Southern Ocean and Deglacial CO_2 Rise, Science, 328, 1147–1151, https://doi.org/10.1126/science.1183627, 2010.

Stickley, C. E., Fuller, M., Kelly, D. C., Nürnberg, D., Pfuhl, H. A., Schellenberg, S. A., Schoenfeld, J., Suzuki, N., Touchard, Y., Wei, W., Williams, G. L., Lara, J., and Stant, S. A.: Proceedings of the Ocean Drilling Program, 189 Scientific Results, edited by: Exon, N. F., Kennett, J. P., and Malone, M. J., Ocean Drilling Program, https://doi.org/10.2973/odp.proc.sr.189.2004, 2004.

Stockmarr, J.: Tables with spores used in absolute pollen analysis, Poll. Spor., 13, 615–621, 1971.

Taylor, K. W. R., Huber, M., Hollis, C. J., Hernandez-Sanchez, M. T., and Pancost, R. D.: Re-evaluating modern and Palaeogene GDGT distributions: Implications for SST reconstructions, Global Planet. Change, 108, 158–174, https://doi.org/10.1016/j.gloplacha.2013.06.011, 2013.

Teruel, O., Rosell-Melè, A., and Penalva-Arias, N.: Global patterns of oceanic dust deposition during Pliocene-Pleistocene transitions, EGU General Assembly 2021, online, 19–30 Apr 2021, EGU21-10616, https://doi.org/10.5194/egusphere-egu21-10616, 2021.

Thöle, L. M., Amsler, H. E., Moretti, S., Auderset, A., Gilgannon, J., Lippold, J., Vogel, H., Crosta, X., Mazaud, A., Michel, E., Martínez-García, A., and Jaccard, S. L.: Glacial-interglacial dust and export production records from the Southern Indian Ocean, Earth Planet. Sc. Lett., 525, 115716, https://doi.org/10.1016/j.epsl.2019.115716, 2019.

Thöle, L. M., Nooteboom, P. D., Hou, S., Wang, R., Nie, S., Michel, E., Sauermilch, I., Marret, F., Sangiorgi, F., and Bijl, P. K.: An expanded database of Southern Hemisphere surface sediment dinoflagellate cyst assemblages and their oceanographic affinities, J. Micropalaeontol., 42, 35–56, https://doi.org/10.5194/jm-42-35-2023, 2023.

Tiedemann, R., Sarnthein, M., and Shackleton, N. J.: Astronomic timescale for the Pliocene Atlantic $\delta^{18}O$ and dust flux records of Ocean Drilling Program Site 659, Paleoceanography, 9, 619–638, https://doi.org/10.1029/94PA00208, 1994.

Tierney, J. E. and Tingley, M. P.: A Bayesian, spatially-varying calibration model for the TEX86 proxy, Geochim. Cosmochim. Ac., 127, 83–106, https://doi.org/10.1016/j.gca.2013.11.026, 2014.

Toggweiler, J. R., Russell, J. L., and Carson, S. R.: Midlatitude westerlies, atmospheric CO_2, and climate change during the ice ages: Westerlies and CO_2 during the Ice Ages, Paleoceanography, 21, PA2005, https://doi.org/10.1029/2005PA001154, 2006.

Van der Weijst, C. M. H., van der Laan, K. J., Peterse, F., Reichart, G.-J., Sangiorgi, F., Schouten, S., Veenstra, T. J. T., and Sluijs, A.: A 15-million-year surface- and subsurface-integrated TEX_{86} temperature record from the eastern equatorial Atlantic, Clim. Past, 18, 1947–1962, https://doi.org/10.5194/cp-18-1947-2022, 2022.

Venugopal, A. U., Bertler, N. A. N., Severinghaus, J. P., Brook, E. J., Cortese, G., Lee, J. E., Blunier, T., Mayewski, P. A., Kjær, H. A., Carter, L., Weber, M. E., Levy, R. H., Pyne, R. L., and Vandergoes, M. J.: Antarctic evidence for an abrupt northward shift of the Southern Hemisphere westerlies at 32 ka BP, Nat. Commun., 14, 5432, https://doi.org/10.1038/s41467-023-40951-1, 2023.

Weiffenbach, J. E., Dijkstra, H. A., von der Heydt, A. S., Abe-Ouchi, A., Chan, W.-L., Chandan, D., Feng, R., Haywood, A. M., Hunter, S. J., Li, X., Otto-Bliesner, B. L., Peltier, W. R., Stepanek, C., Tan, N., Tindall, J. C., and Zhang, Z.: Highly stratified mid-Pliocene Southern Ocean in PlioMIP2, Clim. Past, 20, 1067–1086, https://doi.org/10.5194/cp-20-1067-2024, 2024.

Westerhold, T., Marwan, N., Drury, A. J., Liebrand, D., Agnini, C., Anagnostou, E., Barnet, J. S. K., Bohaty, S. M., De Vleeschouwer, D., Florindo, F., Frederichs, T., Hodell, D. A., Holbourn, A. E., Kroon, D., Lauretano, V., Littler, K., Lourens, L. J., Lyle, M., Pälike, H., Röhl, U., Tian, J., Wilkens, R. H., Wilson, P. A., and Zachos, J. C.: An astronomically dated record of Earth's climate and its predictability over the last 66 million years, Science, 369, 1383–1387, https://doi.org/10.1126/science.aba6853, 2020.

Yamane, M., Yokoyama, Y., Abe-Ouchi, A., Obrochta, S., Saito, F., Moriwaki, K., and Matsuzaki, H.: Exposure age and ice-sheet model constraints on Pliocene East Antarctic ice sheet dynamics, Nat. Commun., 6, 7016, https://doi.org/10.1038/ncomms8016, 2015.

Yan, Y., Bender, M. L., Brook, E. J., Clifford, H. M., Kemeny, P. C., Kurbatov, A. V., Mackay, S., Mayewski, P. A., Ng, J., Severinghaus, J. P., and Higgins, J. A.: Two-million-year-old snapshots of atmospheric gases from Antarctic ice, Nature, 574, 663–666, https://doi.org/10.1038/s41586-019-1692-3, 2019.

Zhang, Z., Nisancioglu, K. H., and Ninnemann, U. S.: Increased ventilation of Antarctic deep water during the warm mid-Pliocene, Nat. Commun., 4, 1499, https://doi.org/10.1038/ncomms2521, 2013.

Zhang, Z., Li, X., Guo, C., Otterå, O. H., Nisancioglu, K. H., Tan, N., Contoux, C., Ramstein, G., Feng, R., Otto-Bliesner, B. L., Brady, E., Chandan, D., Peltier, W. R., Baatsen, M. L. J., von der Heydt, A. S., Weiffenbach, J. E., Stepanek, C., Lohmann, G., Zhang, Q., Li, Q., Chan-

dler, M. A., Sohl, L. E., Haywood, A. M., Hunter, S. J., Tindall, J. C., Williams, C., Lunt, D. J., Chan, W.-L., and Abe-Ouchi, A.: Mid-Pliocene Atlantic Meridional Overturning Circulation simulated in PlioMIP2, Clim. Past, 17, 529–543, https://doi.org/10.5194/cp-17-529-2021, 2021.

Ziegler, M., Diz, P., Hall, I. R., and Zahn, R.: Millennial-scale changes in atmospheric CO_2 levels linked to the Southern Ocean carbon isotope gradient and dust flux, Nat. Geosci., 6, 457–461, https://doi.org/10.1038/ngeo1782, 2013.

Zonneveld, K. A. F., Marret, F., Versteegh, G. J. M., Bogus, K., Bonnet, S., Bouimetarhan, I., Crouch, E., de Vernal, A., Elshanawany, R., Edwards, L., Esper, O., Forke, S., Grøsfjeld, K., Henry, M., Holzwarth, U., Kielt, J.-F., Kim, S.-Y., Ladouceur, S., Ledu, D., Chen, L., Limoges, A., Londeix, L., Lu, S.-H., Mahmoud, M. S., Marino, G., Matsouka, K., Matthiessen, J., Mildenhal, D. C., Mudie, P., Neil, H. L., Pospelova, V., Qi, Y., Radi, T., Richerol, T., Rochon, A., Sangiorgi, F., Solignac, S., Turon, J.-L., Verleye, T., Wang, Y., Wang, Z., and Young, M.: Atlas of modern dinoflagellate cyst distribution based on 2405 data points, Rev. Palaeobot. Palyno., 191, 1–197, https://doi.org/10.1016/j.revpalbo.2012.08.003, 2013.